High-order conservative semi-Lagrangian finite volume schemes for transport equations

Nanyi Zheng, Xiaofeng Cai, Jingmei Qiu, Jianxian Qiu

University of Delaware

July 24th

Outline

Transport equation

General form:

$$u_t + \nabla_{\mathbf{x}} \cdot (\mathbf{a}(u, \mathbf{x}, t)u) = 0. \tag{1}$$

Examples:

2-D Linear transport equation:

$$u_t + (a(x, y, t)u)_x + (b(x, y, t)u)_y = 0. \tag{2}$$

1D1V Vlasov-Poisson system:

$$f_t + vf_x + E(x, t)f_v = 0, \tag{3}$$

$$E_x = \int_{\mathbb{R}} f(x, v, t)dv - \frac{1}{|\Omega_x|}\int_{\Omega_x}\int_{\mathbb{R}} f(x, v, 0)dvdx. \tag{4}$$

Applications

- Climate modeling

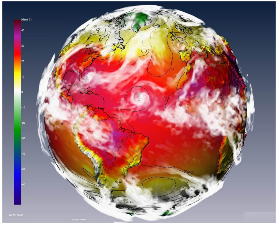

- Plasma application

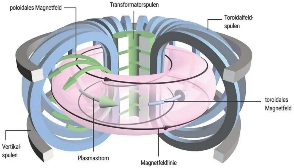

Semi-Lagrangian (SL) schemes

- Semi-Lagrangian (SL) [E. Sonnendrücker 1999, N. Besse 2003, J.-M. Qiu 2010]

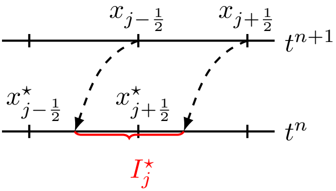

- Splitting-based SL
- Non-splitting SL

Major goals

Introduce two different kinds of SL finite volume (FV) schemes enjoying all the following properties:

- Mass conservation
- High-order accuracy in time and space
- Unconditional stability (large time step)
- Positivity preservation

Outline

1-D SL-FV formulation

Consider a 1-D linear transport equation

$$\frac{\partial u}{\partial t} + \frac{\partial}{\partial x}(a(x,t)u) = 0. \tag{5}$$

We define that $X(x;t)$ represents the characteristic curve emanating from (x, t^{n+1}), i.e. the solution of the following ordinary differential equation (ODE):

$$\begin{cases} dX(t)/dt = a(X(t),t), \\ X(t^{n+1}) = x, \end{cases} \tag{6}$$

An SL-FV scheme is formulated as follow:

$$\frac{1}{\Delta x}\int_{I_j} u(x,t^{n+1})dx = \frac{1}{\Delta x}\int_{I_j^\star} u(x,t^n)dx, \tag{7}$$

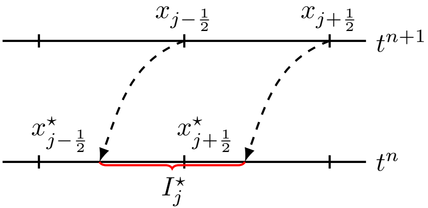

1-D SL-FV-WENO scheme

$$\overline{u}_j^{n+1} = \frac{1}{\Delta x} \int_{\widetilde{I}_j^\star} \mathcal{W}\left(\{\overline{u}_i^n\}\right) dx, \tag{8}$$

where $\mathcal{W}(\cdot)$ represents a piecewise reconstruction polynomial.

1-D WENO-ZQ reconstruction method

$\boxed{\text{The FV solution } \{\overline{u}_i^n\} \xrightarrow{\mathcal{W}} \text{a piecewise } P^4 \text{ polynomial } \widetilde{u}(x)}$

where

$$\widetilde{u}(x) = \widetilde{u}^{(i)}(x) \in P^4(I_i), \quad (x, y) \in I_i, \quad \forall i.$$

Schematics of the reconstruction procedure

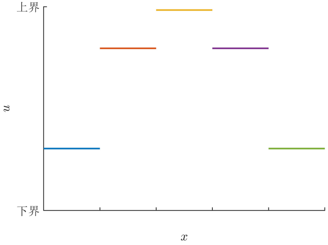

(b) FV solution

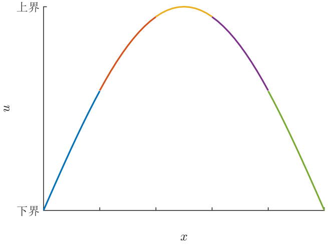

(c) Reconstructed piecewise P^4 polynomial

Splitting-Based SL-FV-WENO Scheme

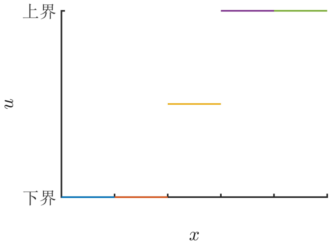

(d) FV solution

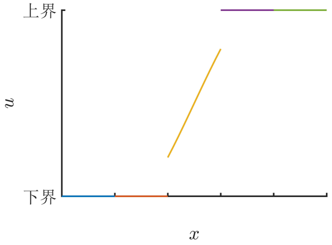

(e) WENO-ZQ reconstruction

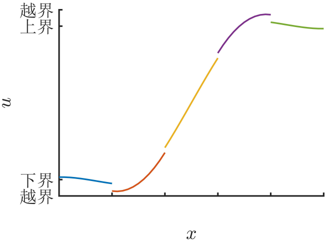

(f) Linear reconstruction

1-D WENO-ZQ reconstruction

The 1-D WENO-ZQ reconstruction polynomial at I_i is defined by

$$\tilde{u}^{(i)}(x) = \omega_1 \left(\frac{1}{\gamma_1} q_1(x) - \frac{\gamma_2}{\gamma_1} q_2(x) - \frac{\gamma_3}{\gamma_1} q_3(x) \right) + \omega_2 q_2(x) + \omega_3 q_3(x), \quad (9)$$

where

- $\{\gamma_l\}$ is a set of positive weights satisfying $\sum_l \gamma_l = 1$,
- $\{\omega_l\}$ is a set of nonlinear weights depending on $\{\gamma_l\}$ and the smoothness of $\{q_l(x)\}$,
- $q_1(x) \in P^4(x)$ is the "big" polynomial constructed based on stencil $\{I_{i-2}, I_{i-1}, I_i, I_{i+1}, I_{i+2}\}$
- $q_2(x) \in P^1(x)$ is the left-biased "small" polynomial constructed based on stencil $\{I_{i-1}, I_i\}$
- $q_3(x) \in P^1(x)$ is the left-biased "small" polynomial constructed based on stencil $\{I_i, I_{i+1}\}$

To be specific:

$$\frac{1}{\Delta x}\int_{I_{i+l}} q_1(x)dx = \overline{u}^n_{i+l},\ l = -2, -1, 0, 1, 2. \tag{10}$$

$$\frac{1}{\Delta x}\int_{I_{i+l}} q_2(x)dx = \overline{u}^n_{i+l},\ l = -1, 0, \tag{11}$$

$$\frac{1}{\Delta x}\int_{I_{i+l}} q_3(x)dx = \overline{u}^n_{i+l},\ l = 0, 1. \tag{12}$$

For more details, see the first WENO-ZQ paper[1].

[1] **J. Zhu and J. Qiu: A new fifth order finite difference WENO scheme for solving hyperbolic conservation laws, J. Comput. Phys., 318 (2016), 110-121..**

High-dimensional splitting-based SL-FV-WENO

$\boxed{\text{1-D SL-FV-WENO scheme}} + \boxed{\text{Dimensional splitting method}}$

Consider the 2-D linear transport equation

$$\frac{\partial u}{\partial t} + \frac{\partial}{\partial x}(a(x,y,t)u) + \frac{\partial}{\partial y}(b(x,y,t)u) = 0. \tag{13}$$

Fourth-order dimensional splitting

$$
\begin{aligned}
&\textbf{stage 1:} \quad \text{evolve} \quad u_t + (au)_x = 0 \quad \text{for} \quad c_1 \Delta t^n, \\
&\textbf{stage 2:} \quad \text{evolve} \quad u_t + (bu)_y = 0 \quad \text{for} \quad d_1 \Delta t^n, \\
&\textbf{stage 3:} \quad \text{evolve} \quad u_t + (au)_x = 0 \quad \text{for} \quad c_2 \Delta t^n, \\
&\textbf{stage 4:} \quad \text{evolve} \quad u_t + (bu)_y = 0 \quad \text{for} \quad d_2 \Delta t^n, \\
&\textbf{stage 5:} \quad \text{evolve} \quad u_t + (au)_x = 0 \quad \text{for} \quad c_3 \Delta t^n, \\
&\textbf{stage 6:} \quad \text{evolve} \quad u_t + (bu)_y = 0 \quad \text{for} \quad d_3 \Delta t^n, \\
&\textbf{stage 7:} \quad \text{evolve} \quad u_t + (au)_x = 0 \quad \text{for} \quad c_4 \Delta t^n
\end{aligned}
\tag{14}
$$

with

$$
\begin{aligned}
&d_1 = d_3 = 1/(2 - 2^{1/3}) \approx 1.3512, \quad d_2 = -2^{1/3}/(2 - 2^{1/3}) \approx -1.7024, \\
&c_1 = c_4 = d_1/2 \approx 0.6756, \quad c_2 = c_3 = (d_1 + d_2)/2 \approx -0.1756.
\end{aligned}
\tag{15}
$$

Nodal-modal exchange for splitting

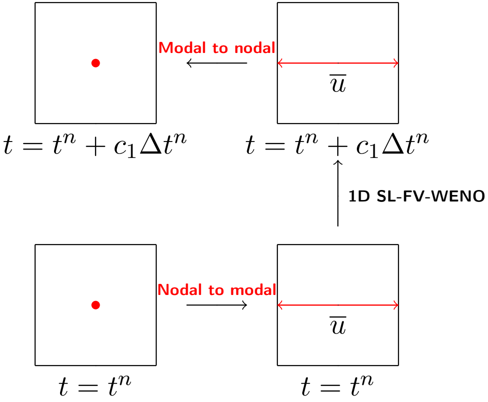

Mass conservation property is not destroyed!

2-D SL-FV formulation

Consider the 2-D linear transport equation

$$\frac{\partial u}{\partial t} + \frac{\partial}{\partial x}(a(x,y,t)u) + \frac{\partial}{\partial y}(b(x,y,t)u) = 0. \tag{16}$$

We define that $(X(x,y;t), Y(x,y;t))$ represents the characteristic curve emanating from (x,y,t^{n+1}), i.e. the solution of the following ordinary differential equations (ODEs):

$$\begin{cases} dX(t)/dt = a(X(t),Y(t),t), \\ dY(t)/dt = b(X(t),Y(t),t), \\ X(t^{n+1}) = x, \\ Y(t^{n+1}) = y. \end{cases} \tag{17}$$

Non-Splitting SL-FV-WENO Scheme

An SL-FV scheme can be formulated as follow:

$$\frac{1}{\Delta x \Delta y} \iint_{I_{i,j}} u(x, y, t^{n+1}) dxdy = \frac{1}{\Delta x \Delta y} \iint_{I^\star_{i,j}} u(x, y, t^n) dxdy, \tag{18}$$

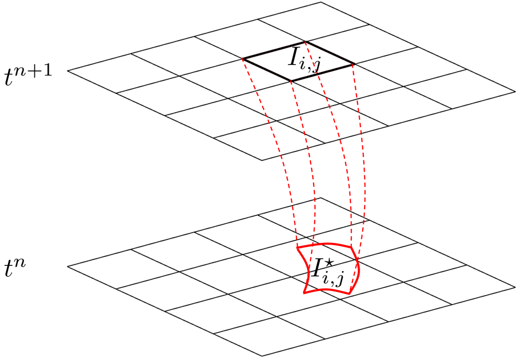

2-D SL-FV-WENO scheme

$$\overline{u}_{i,j}^{n+1} = \frac{1}{\Delta x \Delta y} \iint_{\widetilde{I}_{i,j}^{\star}} \widetilde{u}(x,y) dx dy, \tag{19}$$

where $\widetilde{u}(x,y) := \mathcal{W}^{\text{2D}}(\{\overline{u}_{i,j}^{n}\})$ represents a piecewise reconstruction polynomial.

WENO-ZQ reconstruction method

$$\boxed{\text{The FV solution } \{\overline{u}_{i,j}^{n}\} \xrightarrow{\mathcal{W}^{\mathbf{2D}}} \text{a piecewise } P^3 \text{ polynomial } \widetilde{u}(x,y)}$$

where

$$\widetilde{u}(x,y) = \widetilde{u}^{(i,j)}(x,y) \in P^3(I_{i,j}), \quad (x,y) \in I_{i,j}, \quad \forall (i,j).$$

Reconstructing upstream cells

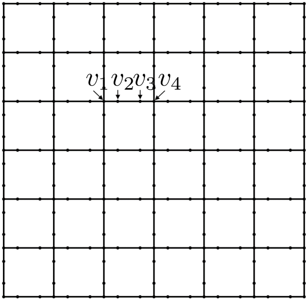

(g) $t = t^{n+1}$

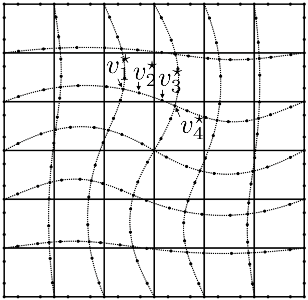

(h) $t = t^n$

step 1 Locate four Gauss-Lobatto-Legendre (GLL) points at each edge of the $\{I_{i,j}\}$.

step 2 For $I^\star_{i,j}$, the characteristic feet $\{v^\star_k\}$ can be obtained by solving the ODEs (17) at $t = t^n$.

step 3 For given curved edge of a characteristic upstream cell, say $I^\star_{i,j}$, there are four characteristic feet, denoted as $\{v^\star_k\}$. By $\{v^\star_k\}$, we interpolate a cubic curve as an edge of $\widetilde{I}^\star_{i,j}$ in parametric form:

$$\begin{cases} x(\xi) = x_a\xi^3 + x_b\xi^2 + x_c\xi + x_d, \\ y(\xi) = y_a\xi^3 + y_b\xi^2 + y_c\xi + y_d, \quad \xi \in [-1, 1]. \end{cases} \tag{20}$$

Clipping

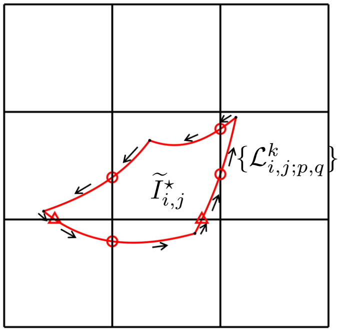

Figure 1: Schematic illustration for the definitions of outer integral segments (left) and inner integral segments (right). The red circles and triangles represent the intersection points of $\widetilde{I}^\star_{i,j}$ and the Eulerian mesh.

Integral strategy

$$
\begin{aligned}
\overline{u}_{i,j}^{n+1} =& \frac{1}{\Delta x \Delta y} \iint_{\widetilde{I}_{i,j}^{\star}} \widetilde{u}(x,y)dxdy \\
=& \frac{1}{\Delta x \Delta y} \sum_{(p,q)} \iint_{\widetilde{I}_{i,j;p,q}^{\star}} \widetilde{u}^{(p,q)}(x,y)dxdy \\
=& \frac{1}{\Delta x \Delta y} \sum_{(p,q)} \int_{\partial(\widetilde{I}_{i,j;p,q}^{\star})} \left[\widetilde{P}^{(p,q)}dx + \widetilde{Q}^{(p,q)}dy\right] \\
=& \sum_{(p,q)} \Bigg\{ \sum_{k} \int_{\mathcal{L}_{i,j;p,q}^{k}} \left[\widetilde{P}^{(p,q)}dx + \widetilde{Q}^{(p,q)}dy\right] \\
& + \sum_{k} \int_{\mathcal{S}_{i,j;p,q}^{k}} \left[\widetilde{P}^{(p,q)}dx + \widetilde{Q}^{(p,q)}dy\right] \Bigg\},
\end{aligned}
\tag{21}
$$

Outline

Theoretical Properties

- **Mass conservation**

$$\sum \overline{u}_{i,j}^{n+1} = \sum \overline{u}_{i,j}^{n}.$$

- **High-order accuracy in time and space**

$$|\overline{u}_{i,j}^{n+1} - \frac{1}{\Delta x \Delta y} \iint_{I_{i,j}} u(x, y, t^{n+1}) dxdy| = O(\Delta x^4).$$

- **Unconditional stability**

$$\|\overline{\mathbf{u}}^{n+1}\|_2 \leq \|\overline{\mathbf{u}}^{n}\|_2.$$

- **Positivity preservation**[2]

$$\overline{u}_{i,j}^{n} \geq 0 \quad \text{for all } i, j, n.$$

[2] X. Zhang, C. W. Shu, On maximum-principle-satisfying high order schemes for scalar conservation laws, Journal of Computational Physics 229 (2010).

Outline

Linear transport simulation

Example 1

(Swirling deformation flow). Consider

$$\begin{aligned} u_t - (2\pi \cos^2(\frac{x}{2}) \sin(y) g(t) u)_x + (2\pi \sin(x) \cos^2(\frac{y}{2}) g(t) u)_y = 0, \\ x \in [-\pi, \pi], \quad y \in [-\pi, \pi], \end{aligned} \tag{22}$$

where $g(t) = \cos(\pi t / T)$ and $T = 1.5$.

Table 1: (Swirling deformation flow). L^2 errors and corresponding orders of accuracy of the non-splitting and splitting-based schemes at $t = 1.5$ with CFL = 10.2.

	Non-splitting		**Splitting**	
mesh	L^2 error	order	L^2 error	order
40×40	6.47E-03	—	1.63E-02	—
80×80	5.82E-04	3.47	2.01E-03	3.02
160×160	4.47E-05	3.70	9.42E-05	4.41
320×320	3.90E-06	3.52	5.39E-06	4.13
640×640	3.28E-07	3.57	3.11E-07	4.12
1280×1280	2.51E-08	3.71	1.50E-08	4.37
2560×2560	3.11E-11	9.66	1.15E-10	7.03
5120×5120	1.37E-12	4.50	2.39E-12	5.59

Numerical Tests

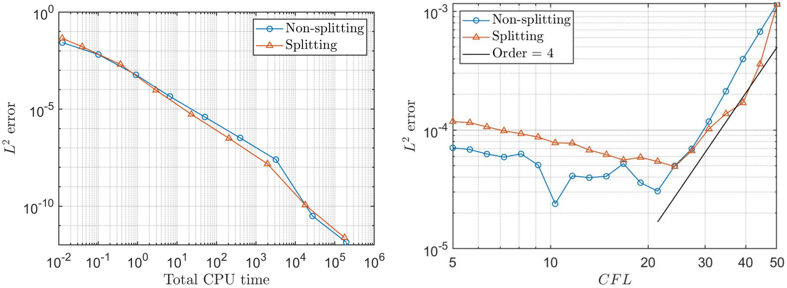

(a) (b)

Figure 2: (Swirling deformation flow). Left: log-log plot of the CPU times vs. the L^2 errors with the same settings in Table 1. Right: log-log plot of the CFL numbers vs. the L^2 errors with a fixed mesh of 160×160 at $t = 1.5$.

Example 2 (Swirling deformation flow)

Consider (22) with the following discontinuous initial condition:

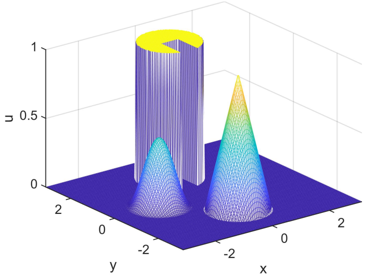

(a) Mesh plot

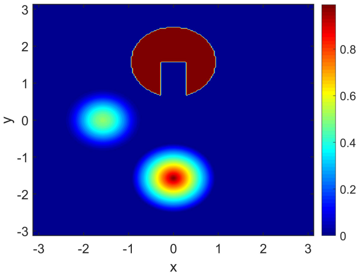

(b) Contour plot

Figure 3: (Swirling deformation flow). Mesh plot and contour plot of the discontinuous initial condition.

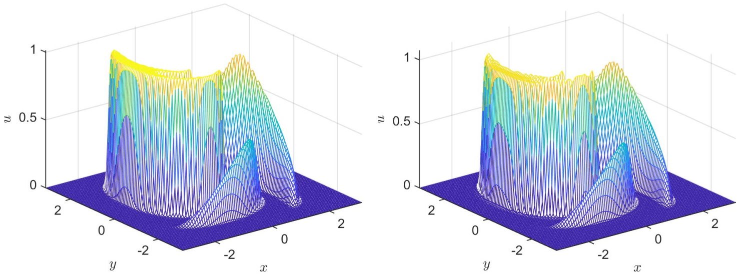

(a) Non-splitting (b) Splitting

Figure 4: (Swirling deformation flow). Mesh plots of the numerical solutions of the two methods with CFL $= 10.2$ at $t = 0.75$.

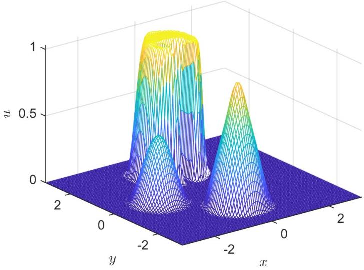

(a) Non-splitting

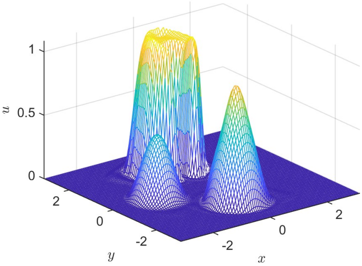

(b) Splitting

Figure 5: (Swirling deformation flow). Mesh plots of the numerical solutions of the two methods with CFL $= 10.2$ at $t = 1.5$.

Nonlinear guiding center Vlasov model

The guiding center Vlasov model describes a highly magnetized plasma in the transverse of a tokamak[3,4]. It can be written as

$$\rho_t + \nabla \cdot \left(\mathbf{E}^{\perp}\rho\right) = 0, \tag{23}$$

$$-\Delta\Phi = \rho, \quad \mathbf{E}^{\perp} = (-\Phi_y, \Phi_x), \tag{24}$$

where $\rho(x, y, t)$ represents the charge density and $\mathbf{E}$ is the electric field.

- $\Delta t = \dfrac{\mathrm{CFL}}{\dfrac{\max\{|E_1|\}}{\Delta x} + \dfrac{\max\{|E_2|\}}{\Delta y}}$.

[3] M. M. Shoucri, A twoâĂŘlevel implicit scheme for the numerical solution of the linearized vorticity equation, International Journal for Numerical Methods in Engineering 17 (2010).

[4] N. Crouseilles, M. Mehrenberger, E. SonnendrÃijcker, Conservative semi-Lagrangian schemes for Vlasov equations, Journal of Computational Physics 229 (2010).

Numerical Tests

Example 3 (Kelvin-Helmholtz instability problem)

Consider the guiding center Vlasov model with initial condition

$$u(x,y,0) = \mathsf{sin}(y) + 0.015\mathsf{cos}(kx), \quad x \in [0,4\pi], \quad y \in [0,2\pi], \tag{25}$$

where $k = 0.5$, and with the periodic boundary condition.

Table 2: (Kelvin-Helmholtz instability problem). L^2 errors and corresponding orders of accuracy of the non-splitting and splitting-based SL-FV WENO schemes for Kelvin-Helmholtz instability problem at $T = 5$ with CFL = 1.

mesh	Non-splitting L^2 error	Non-splitting order	Splitting L^2 error	Splitting order
16×16	3.49E-03	—	2.35E-02	—
32×32	2.64E-04	3.73	1.28E-02	0.88
64×64	1.04E-05	4.66	6.80E-03	0.91
128×128	4.65E-07	4.49	3.51E-03	0.95
256×256	3.12E-09	7.22	1.79E-03	0.97
512×512	8.89E-11	5.14	9.03E-04	0.99

Numerical Tests

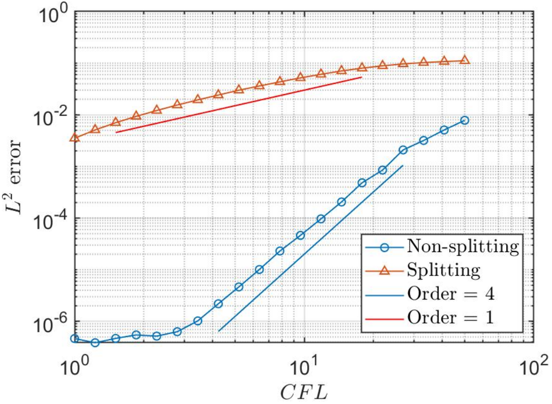

Figure 6: (Kelvin-Helmholtz instability problem). Log-log plot of the CFL numbers vs. the L^2 errors of the two schemes with a fixed mesh of 128×128 for Kelvin-Helmholtz instability problem at $T = 5$.

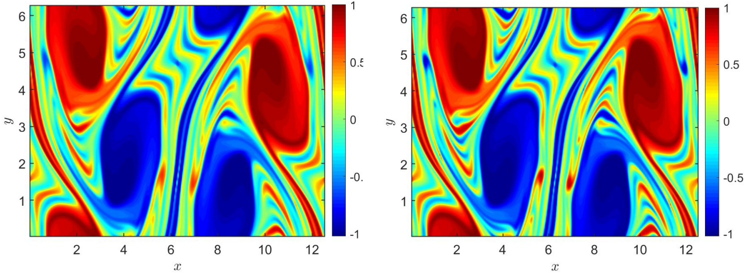

Figure 7: (Kelvin-Helmholtz instability problem). Contour plots of the numerical solution of the non-splitting SL-FV WENO scheme with CFL = 1 (left) and with CFL = 10.2 (right) at $T = 40$.

Numerical Tests

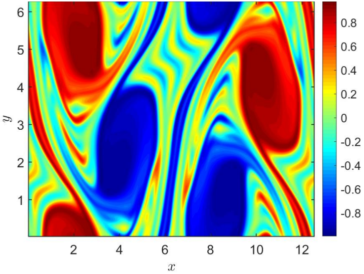

Figure 8: (Kelvin-Helmholtz instability problem). Contour plots of the numerical solution of the splitting-based SL-FV WENO scheme with CFL = 0.1 (left) and CFL = 1 (right) at $T = 40$.

Outline

1. Background
2. Design of the SL-FV-WENO Schemes
3. Theoretical Properties
4. Numerical Tests
5. Concluding Remarks

Concluding Remarks

- The splitting-based SL-FV-WENO scheme is easy to extend to arbitrary high-dimensional problems. However, its accuracy decays to first-order for some nonlinear models.
- The non-splitting SL-FV-WENO scheme shows great potential and seems to be the better one. However, it is extremely difficult to extend to higher-dimensional problems.

Future works

- Higher-dimensional clipping-free non-splitting SL-FV schemes.
- More general models.

Publication:

1. N. Zheng, X. Cai, J.-M. Qiu and J. Qiu: A conservative semi-Lagrangian hybrid Hermite WENO scheme for linear transport equations and the nonlinear Vlasov-Poisson system, *SIAM J. Sci. Comput.*, 43(2021), A3580–A3606. https://doi.org/10.1137/20M1363273.
2. N. Zheng, X. Cai, J.-M. Qiu and J. Qiu: A fourth-order conservative semi-Lagrangian finite volume WENO scheme without operator splitting for kinetic and fluid simulations, *Comput. Methods Appl. Mech. Engrg.*, 395 (2022) 114973. https://doi.org/10.1016/j.cma.2022.114973

Thanks for your attention!